Perturbed-angular-correlation spectroscopy of the fluctuating hyperfine interaction at Cd-donor pairs in silicon: An approach to electronic transitions at impurities in semiconductors

Norbert Achtziger and Wolfgang Witthuhn
Physikalisches Institut der Universität Erlangen-Nürnberg, E. Rommel Straße 1, D-8520 Erlangen, Germany
(Received 28 May 1992)

Cadmium-donor pairs in *n*-type silicon (donors: P, As, Sb) are investigated by perturbed-angular-correlation (PAC) spectroscopy at the probe atom ^{111}In/^{111}Cd. The pairs are formed between ^{111}In and the donors; the hyperfine interaction is measured by PAC directly after the radioactive decay of ^{111}In to ^{111}Cd and thus provides information about the electronic charge distribution around the Cd atom. For each type of donor the PAC spectra reveal two specific electric-field gradients (EFG's). It is demonstrated that these EFG's correspond to two different states of the same atomic configuration (one probe atom and one donor atom). PAC spectra are measured as a function of temperature (280–1100 K) and donor concentration ($\geq 10^{17}$ cm^{-3}) and under the influence of a Schottky contact. Direct evidence for a fluctuating hyperfine interaction is found. The experimental results imply that the Cd-donor pairs form electrically active centers with one energy level close to the center of the band gap. Both relaxation effects initiated by the ^{111}In$\rightarrow^{111}$Cd decay as well as equilibrium fluctuations between the two charge states of the pairs give rise to a time-dependent hyperfine interaction. The ionization probability and the transition rates between different charge states are extracted and are discussed in terms of Schottky-Read statistics. Both energy level and capture cross sections are derived. Within experimental errors, the electronic properties do not depend on the type of donor. The quantitative determination of dynamic properties from PAC spectra is enabled by the calculation of the perturbation function $G(t)$ for a two-state model allowing fluctuations between axially symmetric EFG's of different strength. Some general properties of this function are discussed.

I. INTRODUCTION

Most of the electronic and optical properties of semiconductors are determined by electrically active defects (intrinsic defects or impurities). Even small concentrations (10^{-6} or less) may have a strong influence, and important parameters like conductivity or carrier lifetime can be varied within orders of magnitude by doping the semiconductor with appropriate impurities. The basic property of these defects is the existence of a localized electronic state with an energy level in the band gap. Capture and emission of charge carriers at these levels are important processes: they govern electronic relaxation phenomena and are involved in the dynamic equilibrium at partially occupied levels.

Many electrical and optical methods are available to detect these processes and to measure their rates. All of these methods are working in nonequilibrium conditions; in many cases, a macroscopic transport property (e.g., current and capacitance) is measured which is indirectly sensitive to the impurity transitions via their influence on the electron distribution in the bands. The perturbed-angular-correlation (PAC) spectroscopy, however, is sensitive to the charge distribution around a probe atom on an atomic scale. If such a probe atom is part of an electrically active complex, the charge transition can be observed directly. In this sense, the technique is strictly complementary to classical methods. To achieve a complete description of dynamic effects, the complete PAC theory for fluctuating interaction has to be used. Former PAC studies on electrically active defects[1–4] described dynamic effects only semiempirically, and transition rates could not be derived.

The PAC spectroscopy is able to measure the hyperfine interaction (HFI) of a magnetic field (not discussed here) or an electric-field gradient (EFG) with radioactive probe nuclei which are incorporated into the sample. The EFG tensor can be specified completely; it is an integral quantity ("fingerprint") of the charge distribution very close ($\ll 1$ nm) to the probe atom. In all experiments presented, the probe nucleus ^{111}Cd, originating from the electron capture (EC) decay of ^{111}In, is used. Therefore the trapping and detrapping of the donors at the probe atom is governed by the properties of the indium atom. The EFG, however, is measured at the cadmium nucleus immediately after the decay (within a time window of 0.5 μs), thus yielding information about the electronic structure of the corresponding Cd-donor pairs.

The formation of pairs between acceptors and donors in semiconductors is well understood in principle,[5] though quantitative data, especially for the acceptor indium, are rather poor. In this work, the pair formation between In and the donors D (D=P,As,Sb) is covered only as far as it is necessary for the discussion of the properties of the CdD pairs. From the present experiments, however, quantitative data about the pairing reaction between indium and the donors can be extracted which will be reported elsewhere.[6] For this pair formation study, the results of the present paper have to be taken into consideration properly.

We want to stress that the EFG's which characterize the equilibrium state of CdD pairs (in n-Si) after the ^{111}In decay are also detected after pairing between ^{111m}Cd and the donors.[7] This means that the investigated CdD pairs are formed (among others) between Cd and the donors, too. The apparently more complicated use of ^{111}In($\rightarrow^{111}$Cd) has primarily technical reasons and additionally enables the investigation of electronic relaxation effects after the elementary transmutation.

The contents of the present paper are described briefly below. The detailed presentation of experiments and results is restricted to the donor phosphorus; the behavior of arsenic and antimony is very similar and will be summarized at the end of each section.

The PAC spectra of isochronal annealing experiments clearly reveal two states for each of the CdD pairs (Sec. IV). These two states are assigned to different charge states due to their dependence on temperature and sample doping and their sensitivity to the space-charge region of a Schottky contact (Sec. V). The explanation for the measured effects by the electronic activity of the pairs includes both relaxation phenomena after the indium decay and equilibrium fluctuations of the charge state in the case of a partial occupation of the level. Consequently the hyperfine interaction at the probe nucleus is not static.

As a detailed analysis of PAC spectra requires knowledge of a perturbation function underlying the HFI in question, this function is calculated for fluctuating EFG strength in a two-state model (Sec. II). The basic requirements of this model are rather general; therefore the calculated perturbation function is of general interest and should be applicable to other topics of PAC spectroscopy, as well.

Both ionization probability and the transition rates at the Cd-donor pairs are extracted from the spectra; they are discussed in terms of ordinary semiconductor statistics and basic electron parameters of the pairs are derived (Sec. VI).

II. PAC THEORY: PERTURBATION FUNCTION FOR FLUCTUATING EFG STRENGTH

In the theory of the perturbed angular correlation of γ rays, the influence of extranuclear fields can be separated in the form of a perturbation function $G(t)$ from other factors depending on nuclear properties of the probe atom.[8] As the experiments directly yield (besides a constant factor) this perturbation function, it is the link between experiment and theory in PAC spectroscopy. $G(t)$ contains all the information which is of interest for solid-state spectroscopy.

Analytical expressions for $G(t)$ in the case of electrical HFI are known only for static interaction and some special cases of fluctuating interaction.[9,10] A general theory of the perturbation function $G(t)$ with only slight restrictions on the dynamic process has been given by Winkler and Gerdau.[11] Based on this theory, we have calculated $G(t)$ for the nuclear spin $I=\frac{5}{2}$ (this holds for the most important PAC-probe nuclei) and for a simple two-state model which can be solved analytically.

To specify the model, first the static electrical hyperfine interaction has to be introduced: the quantity which specifies the HFI between a charge distribution and a nucleus is the tensor of the electric-field gradient (EFG). It is defined as the traceless part of the second spatial derivative of the electrostatic potential at the site of the probe nucleus. As usual, it is described by its largest component V_{zz} and the asymmetry parameter $\eta=(V_{xx}-V_{yy})/V_{zz}$, where the V_{ii} are Cartesian components in the principal axes system. Instead of V_{zz}, the (quadrupole) coupling constant ν_Q or the interaction frequency ω_0 is frequently used to specify the strength of the EFG. These quantities are related by

$$\nu_Q=eQV_{zz}/h=\frac{10}{3\pi}\omega_0 , \tag{1}$$

where Q is the quadrupole moment of the nucleus ($I=\frac{5}{2}$). For static interaction with an axially symmetric EFG (i.e., $\eta=0$) the perturbation function is a sum of cosine terms with an integer frequency ratio:

$$G(t)=\sum_{n=0}^{3} S_n\cos(n\omega_0 t) ; \quad \left[\sum_{n=0}^{3} S_n=1\right] . \tag{2}$$

The coefficients S_n depend on the orientation of the EFG's principal axes system only.

The dynamic model is specified by the following assumptions.

(1) There are two states $|1\rangle$ and $|2\rangle$ of the charge distribution around the probe atom, resulting in two EFG's and no magnetic interaction. Both EFG tensors are axially symmetric ($\eta=0$) and have an identical principal-axes system, but different strengths (coupling constants $\nu_Q^{(1)}$ and $\nu_Q^{(2)}$). To avoid ambiguities, $\nu_Q^{(1)}\geq|\nu_Q^{(2)}|$ is presupposed.

(2) The (first-order) transitions between the two states are characterized by

$$\frac{dn_1}{dt}=-\gamma_1 n_1+\gamma_2(1-n_1) , \tag{3}$$

where $n_1(t)$ is the probability of state $|1\rangle$, γ_1 the rate of the transition $|1\rangle\rightarrow|2\rangle$, and γ_2 the rate for $|2\rangle\rightarrow|1\rangle$. Such a system has an equilibrium probability p_1 for being in state $|1\rangle$,

$$p_1=\gamma_2/\gamma , \quad \text{with} \quad \gamma=(\gamma_1+\gamma_2) , \tag{4}$$

and shows an exponential relaxation to this value with a time constant $(1/\gamma)$. Any pair of the parameters γ, γ_1, γ_2, and p_1 can be used to describe the equilibrium kinetics completely. In nonequilibrium conditions, the parameter $p_{1_0}\equiv n_1(t=t_0)$ is additionally used to describe the probability of the state $|1\rangle$ at the time t_0 of the emission of the first gamma ray, i.e., the time zero of the HFI.

The calculation and discussion of the resulting $G(t)$ formula is considerably simplified by introduction of two dimensionless parameters: The (inverse) relative difference of the two EFG's is described by

$$\xi\equiv\frac{\nu_Q^{(1)}+\nu_Q^{(2)}}{\nu_Q^{(1)}-\nu_Q^{(2)}}>0 . \tag{5}$$

For a given system (i.e., fixed EFG's), ξ is a constant.

The "dynamic parameter" Γ_0 normalizes the total transition rate γ to the relevant PAC time scale given by the difference Δ of the interaction frequencies:

$$\Gamma_0 \equiv \frac{\gamma}{\Delta} \geq 0; \quad \Delta \equiv \omega_0^{(1)} - \omega_0^{(2)} = \frac{3\pi}{10}(\nu_Q^{(1)} - \nu_Q^{(2)}) > 0 \ . \tag{6}$$

The perturbation function is calculated by solving the eigenvalue problem of the general theory[11] and some straightforward calculations.[12] The result is

$$G(t) = S_0 + \sum_{n=1}^{3} S_n W\left[\frac{\Gamma_0}{n}, p_1, p_{1_0}, \xi, \frac{n\Delta}{2}t\right] , \tag{7}$$

where for the case $(\Gamma, p_1) \neq (1, \frac{1}{2})$ each of the three partial waves W is given by

$$W(\Gamma, p_1, p_{1_0}, \xi, \tau) = \sum_{j=1}^{2} \Xi_j \exp(-\lambda_j \tau)\cos(\Omega_j \tau + \phi_j) \ . \tag{8}$$

The coefficients of these damped and phase-shifted cosine waves are

$$\Xi_j(\Gamma, p_1, p_{1_0}) = \mathrm{Abs}[U_j(\Gamma, p_1, p_{1_0})] \ , \quad \in [0, \infty] \tag{9}$$

$$\phi_j(\Gamma, p_1, p_{1_0}) = -\mathrm{Arg}[U_j(\Gamma, p_1, p_{1_0})] \ , \quad \in [-\pi, +\pi] \tag{10}$$

$$\lambda_j(\Gamma, p_1) = \Gamma + \epsilon_j \mathrm{Re}[\sqrt{r(\Gamma, p_1)}] \ , \quad \in [0; 2\Gamma] \tag{11}$$

$$\Omega_j(\Gamma, p_1, \xi) = \xi + \epsilon_j \mathrm{Im}[\sqrt{r(\Gamma, p_1)}] \ , \quad \in [\xi - 1; \xi + 1] \ , \tag{12}$$

Abs, Arg, Re, and Im denote absolute value, phase, real, and imaginary parts of the complex quantities

$$U_j(\Gamma, p_1, p_{1_0}) = \tfrac{1}{2}\left[1 - \epsilon_j \frac{\Gamma + i(1 - 2p_{1_0})}{\sqrt{r(\Gamma, p_1)}}\right] , \tag{13}$$

$$r(\Gamma, p_1) = \Gamma^2 - 1 + 2i(1 - 2p_1)\Gamma \ , \tag{14}$$

with the conventions

$$\epsilon_1 \equiv 1 \ , \quad \epsilon_2 \equiv -1, \quad \mathrm{Re}(\sqrt{z}) \geq 0 \quad \text{for } z \in \mathbb{C} \ . \tag{15}$$

For $(\Gamma, p_1) = (1, \frac{1}{2})$, W cannot be expressed in the form of Eq. (8), as the amplitudes Ξ_j are diverging. In this case, W is given by

$$W(1, \tfrac{1}{2}, p_{1_0}, \xi, \tau) = \exp(-\tau)[(1 + \tau)\cos(\xi\tau) + (1 - 2p_{1_0})\tau \sin(\xi\tau)] \ . \tag{16}$$

In the following, general properties of the dynamic perturbation function will be discussed. The strongest effect of the fluctuating HFI on $G(t)$ occurs for $\Gamma_0 \sim 1$. As the three partial waves W are formally identical, but differ in their dynamic parameter $\Gamma = \Gamma_0/n$, all characteristic effects showing up in each partial wave for a certain value of Γ [e.g., phase shifts and frequency splitting (see below)] do not occur at the same value of Γ_0 (or γ), but are shifted to higher transition rates in the second and especially third partial waves.

The properties of this perturbation function will be discussed in two important cases.

A. Thermal equilibrium ($p_1 = p_{1_0}$)

In this case, $G(t)$ depends on the two dynamic parameters Γ_0 and p_1 only. Calculated $G(t)$ functions and their cosine Fourier transforms are shown in Fig. 1; three limiting cases are discussed.

1. $\Gamma_0 \ll 1$, *"quasistatic domain"*

For $\Gamma_0 = 0$, $G(t)$ consists of two fractions with a static perturbation function for each fraction. With increasing Γ_0 this simple function is slightly modified: all three harmonics of each fraction will be damped with the same time constant, and the modulation frequencies of both fractions shift slightly toward each other:

$$G(t) = S_0 + \sum_{j=1}^{2} p_j \exp[-\gamma(1 - p_j)t] \times \sum_{n=1}^{3} S_n \cos\left[\left[n\omega_0^{(j)} - \epsilon_j \frac{\omega'}{n}\right]t\right] , \tag{17}$$

with

$$\omega' = \frac{\gamma^2}{\Delta} p_1 p_2 \ , \quad (p_2 \equiv 1 - p_1) \ . \tag{18}$$

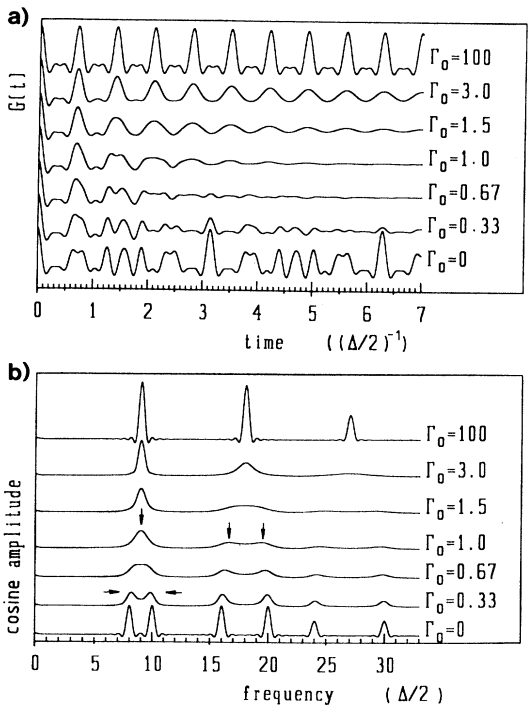

FIG. 1. (a) Calculated perturbation function $G(t)$ and (b) corresponding cosine-Fourier spectra for thermal equilibrium ($p_1 = p_{1_0}$) at different values of the dynamic parameter Γ_0. The model parameters are $p_1 = 50\%$ and $\xi = 11$ (i.e., $\nu_Q^{(1)} = 1.2\nu_Q^{(2)}$); the coefficients S_n are chosen to be $S_1 = S_2 = 0.4$ and $S_3 = 0.2$. The arrows mark typical dynamical effects and are explained in the text.

Because of $\omega' \ll \Delta$, the frequency deviation from the static values $\omega_0^{(j)}$ is very small. In Fig. 1, the frequency shift is marked by arrows at the Fourier spectrum for $\Gamma_0=0.33$.

2. $\Gamma_0 \gg 1$, *"fast fluctuation domain"*

This case is analogous to the well-known motional narrowing effect. Except for an exponential damping factor,[13] $G(t)$ is identical to the perturbation function of one static EFG whose strength is the average of the two single EFG's, weighted by the probabilities p_1 and $p_2=1-p_1$:

$$G(t)=\sum_{n=0}^{3} S_n \cos(n\omega t)\exp(-n^2\delta t) , \tag{19}$$

with

$$\omega=(\omega_0^{(1)}p_1+\omega_0^{(2)}p_2) , \quad p_2\equiv 1-p_1 , \tag{20}$$

$$\delta=\frac{\Delta^2}{\gamma}p_1p_2 . \tag{21}$$

The damping vanishes in the limit $\Gamma_0 \to \infty$. Apart from the damping ratio of the three harmonics (1:4:9 instead of 1:2:3), the $G(t)$ function is the same as for one single EFG with a static (Lorenz) EFG distribution; this function had been used empirically in former studies in the fast fluctuation regime.[2,3] The strong damping of the higher partial waves is visible in the $G(t)$ function for $\Gamma_0=3$ in Fig. 1: only the $n=1$ wave, i.e., a single (damped) cosine function, survives after a few modulations.

3. $\Gamma_0 \sim 1$, *"intermediate domain"*

In this transition region between nearly static behavior and fast fluctuations, strong phase shifts and damping can occur in the $G(t)$ function. Obvious modulations in $G(t)$ occur only if one of the two states dominates (i.e., p_1 is close to 0 or 1) or if the strength of the EFG's is not too different (i.e., $\xi \gg 1$, as in Fig. 1). Otherwise, with increasing Γ_0, the two superpositioned modulations for $\Gamma_0 \ll 1$ are completely wiped out for $\Gamma_0 \sim 1$ before the modulation of the fast fluctuation regime shows up.

The typical effect of the different dynamic parameters Γ of the three partial waves mentioned above is visible in the Fourier spectra of Fig. 1 for $\Gamma_0=1$: The first partial wave ($n=1, \Gamma=\Gamma_0=1$) exhibits only one damped frequency, while the second and third partial waves ($\Gamma=\Gamma_0/n<1$) still show two separate frequencies.

B. Nonequilibrium conditions (i.e., $p_{1_0} \neq p_1$)

An example of this case is illustrated in Fig. 2. The arbitrarily chosen parameters $p_1=1$ and $p_{1_0}=0.5$ describe a system with a (static) equilibrium state $|1\rangle$ and an initial occupation of 50% for both states. For $\Gamma_0=0$ (i.e., zero transition rate) the initial state is conserved and the perturbation function corresponds to two static EFG's (each populated by 50%). With increasing Γ_0, the modulation of the nonequilibrium state $|2\rangle$ is damped (Fig. 2, $\Gamma_0=0.03$). The modulation corresponding to the equilibrium state $|1\rangle$ is markedly influenced for $\Gamma_0 \geq 0.3$: the asymmetry of the modulation pattern and of the Fourier peaks (see arrows in Fig. 2) indicates a phase shift with respect to pure cosine waves. For further increasing Γ_0, the phase shifts disappear, the modulation amplitude increases, and finally ($\Gamma_0 \geq 10$) the spectra correspond to the EFG of the equilibrium state, i.e., the initial state is irrelevant if the relaxation rate is high enough.

For the purpose of fitting experimental spectra by this theoretical function $G(t)$, the values of $\nu_Q^{(1)}$ and $\nu_Q^{(2)}$ should be known and kept fixed. Even if both EFG's can be measured in a static state by choosing proper experimental conditions, the relative sign of $\nu_Q^{(1)}$ and $\nu_Q^{(2)}$ is unknown, as the standard γ-γ PAC is not sensitive to the sign of a static EFG component. In the context of the dynamic theory, however, the sign is important. In general, this ambiguity cannot be overcome without further assumptions.

III. EXPERIMENTAL TECHNIQUE

For a general description of the PAC spectroscopy, we refer to the literature; both detailed descriptions[8,14] as well as reviews concentrating on solid-state spectroscopy[9,15] and especially on semiconductors[16,17] are available.

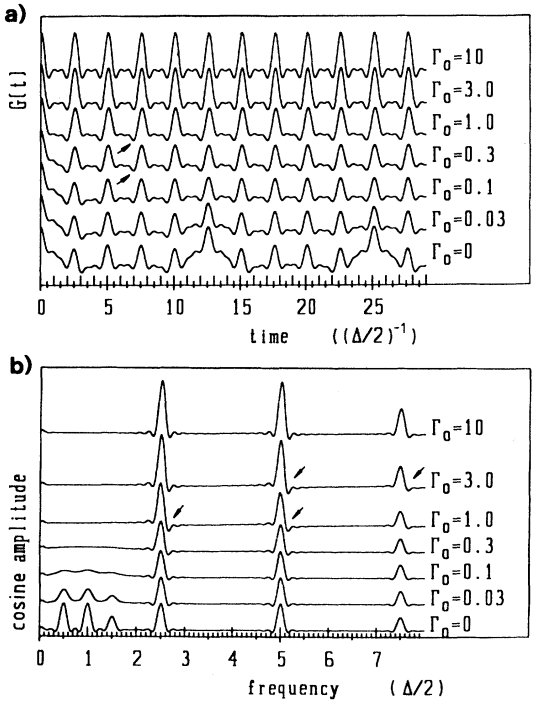

FIG. 2. (a) Calculated perturbation function $G(t)$ and (b) corresponding cosine-Fourier spectra for a relaxation process to static equilibrium at different values of the dynamic parameter Γ_0. The model parameters are $p_{1_0}=50\%$, $p_1=100\%$, and $\xi=1.5$ (i.e., $\nu_Q^{(1)}=5\nu_Q^{(2)}$); for the coefficients S_n, see Fig. 1. The arrows mark typical dynamical effects and are explained in the text.

Here we give only a very short description, valid for the probe atom ^{111}In/^{111}Cd and our experimental setup. The observed quantity is the angular correlation of the two γ quanta of a γ-γ cascade in the ^{111}Cd nucleus. The hyperfine interaction (HFI) between extranuclear fields and the intermediate state of this cascade (nuclear spin $I=\frac{5}{2}$, $T_{1/2}=84$ ns) results in a time dependence of this angular correlation which is recorded by time-differential detection of the γ quanta. The coincidence spectra are combined by a standard procedure, which essentially singles out the time dependence and eliminates nuclear and experimental details to a standard $R(t)$ spectrum. It can be described by

$$R(t)=A_{\text{eff}}G(t)=A_{\text{eff}}\sum_i f_i G^{(i)}(t)\ , \quad \sum_i f_i=1\ , \tag{22}$$

where $A_{\text{eff}}=A_{22}Q=-0.125(5)$ (A_{22} is an anisotropy constant and Q is a geometrical factor depending on detector geometry) and $G(t)$ is the perturbation function which contains all the information about the HFI [$G(t)=1$ for zero HFI]. The second part of the equation applies if different fractions f_i of probe atoms are exposed to different types or strengths of the HFI, each described by its perturbation function $G^{(i)}(t)$. If the correct $G^{(i)}(t)$ is used, the amplitude of a modulation therefore directly yields the corresponding fraction f_i. As $G(t)$ in many cases consists of cosine terms, the cosine-Fourier transform of the experimental $R(t)$ spectra is a practical tool and is usually the first step in the data evaluation. The type of HFI has to be deduced from general properties of the experimental spectra and, finally, quantitative data are derived by fitting Eq. (22) to the spectra. Here we will mainly concentrate on the fraction $f_{\text{Cd}D}$ of probe atoms involved in a CdD pair. The rest of the probe atoms are exposed to zero EFG (fraction f_0) and (especially in ion-implanted samples) to a strong, nonuniform HFI which cannot be resolved. These two fractions result in a nonmodulated contribution to the spectra which thus can easily be separated from the modulations caused by the CdD pairs.

The EC decay of ^{111}In leads to a highly excited Cd atom[8] (with a hole in the K shell). The relaxation of the inner shells is finished before the $\gamma\gamma$ cascade starts (the mean lifetime of the initial state of the cascade is 0.15 ns) and consequently has no influence. Valence electrons, however, and hence the electronic state of the impurity in the semiconductor, may still be affected, causing at least a fractional population of nonequilibrium states. In this context, the PAC state of ^{111}Cd offers an important check: besides the population via EC decay of ^{111}In, it can also be populated by an isomeric transition from the metastable $11/2^-$ level (^{111m}Cd, $T_{1/2}=49$ min) of ^{111}Cd. In this case, the electron shell is unaffected.

All experiments were performed in n-type silicon. With a few exceptions listed below, homogeneously n-doped material (P, As, Sb) was used, and the ^{111}In atoms were incorporated by means of the silicon direct-bonding process[18,2] (SDB): two polished silicon wafers were hydrophilized by a dip in cholin and ^{111}In was applied to one of them. After the wafers were fit together, they stuck together firmly by adhesion. During a subsequent high-temperature treatment (12 h at 1200 K and 24 h at 1500 K), the wafers were bonded and the ^{111}In atoms diffused from the interface into the bulk, resulting in an approximately 10-μm-wide indium profile with a maximum concentration of about 10^{15} cm^{-3}. The donor concentrations were at least two orders of magnitude higher (10^{17} to 3×10^{19} cm^{-3}) and were derived from the room-temperature conductivity. Ion implantations (projected range approximately 160 nm) of both donors and probe atoms were used for the heaviest doped samples and for the Schottky diode experiments only, followed by conventional furnace annealing at 800, 1000, and 1200 K for $\frac{1}{2}$-h each.

IV. INDIUM-DONOR PAIR FORMATION

The formation of pairs (or complexes) of impurities in semiconductors requires both an attractive interaction between them and a sufficiently high mobility of at least one of the atoms. For acceptor-donor pairing, the first condition is fulfilled by the Coulomb attraction of the charged impurities, and the second condition requires a temperature of approximately 1000 K (in silicon), in detail depending on the concentration and diffusivity of the atoms. Therefore the pairing process is investigated by annealing experiments; the PAC spectra were measured at room temperature. The detailed description of the present experiments is restricted to the donor phosphorus.

Figure 3 shows PAC spectra of ^{111}In/^{111}Cd probe

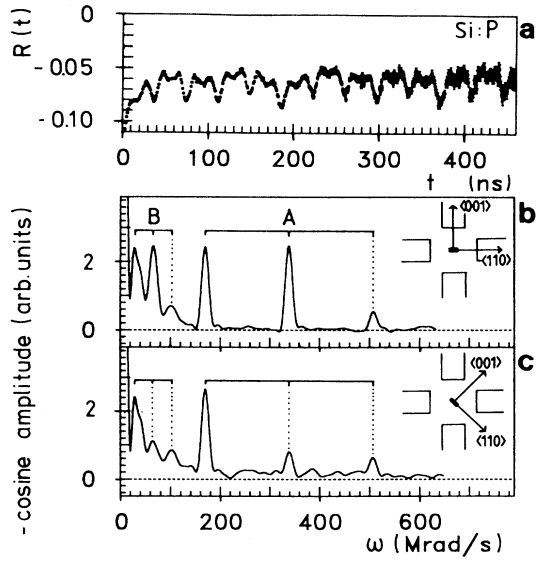

FIG. 3. PAC spectrum (a) and cosine-Fourier spectra (b) and (c) of ^{111}In/^{111}Cd probe atoms in Si:P ($N_D=8\times10^{17}$ cm^{-3}) after a temper process at 1000 K for 2 h, measured at 293 K. The PAC spectrum is a superposition of two modulations; in the Fourier spectra two corresponding triplets of frequencies are visible. Each modulation is due to an electric hyperfine interaction with an axially symmetric EFG. In (c), the detector position relative to the crystal axes is different from (a) and (b). The resulting difference of the partial amplitudes [S_n coefficients in Eq. (2)] within each triplet proves (together with further measurements) the ⟨111⟩ orientation of the z axis of both EFG's.

atoms in Si:P (donor concentration $N_D = 8 \times 10^{17}$ cm^{-3}) after a temperature treatment at 1000 K for 2 h. The $R(t)$ spectrum is the superposition of two modulations labeled A and B. Each of them corresponds to a triplet of frequencies in the Fourier spectrum. Except for a slight damping of modulation B, both modulations *can be* described by a static HFI with an EFG which is axially symmetric around the ⟨111⟩ crystal axes. The EFG strengths (expressed as coupling constants) are $\nu_Q^{(A)} = 180$ (1) MHz and $\nu_Q^{(B)} = 36$ (1) MHz. These EFG's have already been reported by Swanson and Wichert.[19,20] Their assignment of EFG A to a close pair consisting of one probe atom and one P atom is based on the axial symmetry of the EFG and on its dependence on N_D and is confirmed by the present experiments. Here we will show that EFG B belongs to the same pair as well.

In order to quantify the occurrence of the two EFG's empirically, the spectra *can be* described by the fractions f_A and f_B of the probe atoms exposed to EFG's A and B (assumed to be static and thus neglecting the slight damping of modulation B) and the fraction f_0 of unperturbed (i.e., unpaired) probe atoms. In Fig. 4, these fractions are shown during an isochronal annealing sequence of a Si:P sample ($N_D = 10^{18}$ cm^{-3}). The initial temper process at 1215 K followed by a fast cooling of the sample ($\sim 10^3$ K/s) was performed in order to dissolve (as far as possible) those pairs which were formed during a slow cool after sample preparation (SDB process at 1500 K). The data clearly demonstrate that both EFG's are formed and dissolved simultaneously, and that the fraction f_0 is reduced if the EFG's are present.

In samples with a lower donor concentration ($N_D = 10^{17}$ cm^{-3}), the fractions f_A and f_B are reduced (because less pairs are formed), but the ratio $f_A/f_B = 1.3$ (± 0.2) is still the same. In several similar annealing experiments, this ratio turns out to be insensitive to variations of annealing temperature, annealing time (1–20 h), cooling rate ($1-10^3$ K/s), and donor concentration ($10^{17}-10^{18}$ cm^{-3}). This fact implies that both EFG's are due to the same type of atom (i.e., a P atom) trapped at the ^{111}In atom. Otherwise, a difference in the formation kinetics or stability of the pairs and thus in the experimental results should be expected. Therefore the two EFG's must correspond to two different states of the CdP pair.

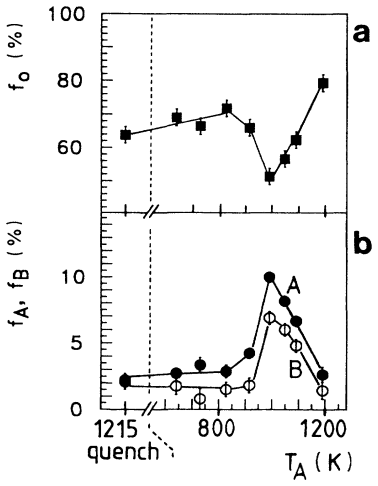

FIG. 4. Empirical description of a pair formation experiment: fractions of probe atoms exposed different EFG's as a function of the annealing temperature (holding time 2 h): (a) fraction f_0 with zero EFG, i.e., unpaired probe atoms; (b) fractions f_A and f_B exposed to static EFG's A and B.

There is only one deviation from the general f_A/f_B ratio: for $N_D > 2 \times 10^{18}$ cm^{-3}, modulation B is not observed (see Fig. 7 and Ref. 20). This fact will be explained by the internal dynamics of the CdP pair (Sec. VI D), and thus does not contradict the assignment of both EFG's to the CdP pair.

The present assignment, which is directly connected to the simultaneous existence of both EFG's, contradicts the statement of Swanson and Wichert that, in their isochronal annealing experiment between 500 and 800 K, EFG B exists exclusively.[20] This interpretation, however, is based on a weakly structured, damped pattern in their spectra, and thus the assignment to the well-defined EFG B is not certain. Their spectra in this range of temperature may just as well be explained by the damage that follows the implantation of the probe atoms. In the present experiments, the annealing program starts from a well-annealed sample with a fraction f_0 of 65% of unperturbed probe atoms, instead of $f_0 \sim 0$ after the implantation, and thus offers a much better starting point for a study of the pair formation process.

As a summary of all pair formation experiments, the other donors As and Sb can be included as well: at approximately 1000 K, close pairs between ^{111}In and one donor atom are formed (for details of the temper process, see Table I). If N_D is below a certain critical value (3×10^{18} cm^{-3} for P, close to 10^{19} cm^{-3} for As and Sb), the PAC spectra measured at room temperature reveal two EFG's (Table II), which represent two different states of the corresponding CdD pair (D = P,As,Sb).

V. EXPERIMENTS ON Cd-DONOR PAIRS

In this section, we will concentrate entirely on the influence of measuring conditions on the PAC spectra in order to study the nature of the two different states of each CdD pair which were identified in the preceding section. The formation of the pairs is of course the first step in these experiments; the relevant parameters are summarized in Table I. The presentation of experiments will again be restricted to the donor phosphorus.

A. Variation of temperature and donor concentration

PAC spectra of CdP pairs in Si were taken for three different phosphorus concentrations between room temperature and a maximum temperature of 1100 K which is limited by the thermal stability of the initially formed InP pairs. All effects described in this section are completely reversible with temperature, provided a temperature of 1000 K is not exceeded. At $T > 1000$ K (according to Sec. IV), the pairs dissociate, and therefore the modulation amplitude of the spectra decreases irreversibly. Fre-

TABLE I. Parameters of sample preparation. "SDB" denotes the silicon direct bonding process (with ^{111}In in the interface) and "IMP" denotes ^{111}In implantation (400 keV). The listed pair formation processes were used in the experiments described in Sec. V A; the influence of the holding time was not investigated systematically in those cases where a value of less than 20 h is given.

n doping	^{111}In doping	Pair formation process (temperature, holding time)
P 10^{17} cm^{-3} homogeneous	SDB	1000 K, 15 h, plus slow cooling to 900 K within 33 h
P 8×10^{17} cm^{-3} homogeneous	SDB, IMP	1000 K, 5–20 h
P 10^{18} cm^{-3} homogeneous	SDB	(see Sec. IV)
P 2.5×10^{14} cm^{-2} implanted, $E=140$ keV	IMP	1045 K, 1 h
As 6×10^{18} cm^{-3} homogeneous	SDB	1100 K, 2 h
	IMP	1000 h, 10 h
Sb 1.6×10^{18} cm^{-3} homogeneous	SDB	1000 K, 110 h
Sb 2.2×10^{18} cm^{-3} homogeneous	SDB	1000 K, 90 h
Sb 10^{15} cm^{-2} implanted, $E=350$ keV	IMP	1000 K, 3 h

quency and damping of the modulations, however, can be studied up to 1100 K, where the fraction f_{CdD} runs below the detection limit. The influence of the pair formation process on measurements at high temperature was additionally checked by long-time annealing experiments (20 h, 900–1000 K) simulating the duration of a PAC measurement. These experiments establish a safe lower limit of 910 K; below this value the fraction f_{CdP} is constant.

The donor concentrations were 10^{17} cm^{-3} and 8×10^{17} cm^{-3} in homogeneous doped SDB samples and $N_D > 10^{18}$ cm^{-3} in a sample produced by P implantation (140 keV, 2.5×10^{14} cm^{-2}, annealed at 1220 K for $\frac{1}{2}$ h) and subsequent ^{111}In implantation (see Table I). In Sec. VI D, the donor concentration of this implanted sample will be determined to 3×10^{18} cm^{-3}.

Some PAC spectra for $N_D=8\times10^{17}$ cm^{-3} at temperatures between 287 and 1023 K are shown in Fig. 5. The spectrum at room temperature is essentially identical to that shown in Fig. 3; it consists of two modulations A and B (B is slightly damped) which can be ascribed to the two EFG's A and B already specified in Sec. IV. With increasing temperature, the spectra change substantially. Taking into account all measured samples (6) and temperatures T ($280\le T\le1000$ K), the following effects are found.

(a) Modulation B vanishes above 450 K; up to this limit the frequency is constant.

TABLE II. Quadrupole coupling constants (absolute values) of the EFG's of the three cadmium-donor pairs at room temperature. All EFG's are axially symmetric around the equivalent ⟨111⟩ crystal axes. The sign of the coupling constants cannot be measured by the standard γ-γ PAC. The interpretation of the experiments in terms of the proposed model favors an identical sign of the coupling constants for both EFG's.

Pair	$\nu_Q^{(1)}$/MHz	$\nu_Q^{(2)}$/MHz
CdP	180	36
CdAs	231	83
CdSb	271	129

(b) The frequency of modulation A strongly decreases for $T\ge700$ K. To describe this effect quantitatively, the basic frequency ω_A of this modulation (the first peak of the frequency triplet) is depicted in Fig. 6 as a function of temperature. The data exhibit a steplike shape.

(c) In the temperature range where the step in the $\omega_A(t)$ curve occurs, the spectra are considerably damped. At the highest temperatures this damping is reduced again.

(d) The amplitude of modulation A is constant up to 500 K and strongly increases between 500 and 700 K by a factor of 2.5 (±0.5). Above 700 K, it is constant up to the temperature limit set by the pair dissociation.

(e) Around 500 K, the modulation pattern is asymmetric, as indicated by the arrows in Fig. 5. In the corresponding Fourier spectrum, this is reflected by an asymmetric peak. This observation implies a phase shift of at least one partial wave of the modulation relative to a cosine function. This effect is of great importance, since for static interaction [see Eq. (2)] phase shifts cannot occur.

(f) The fraction f_0 of unperturbed probe atoms is constant below the dissociation limit (1000 K).

Analogous experiments in samples with a lower P concentration of $N_D=10^{17}$ cm^{-3} exhibit very similar characteristics of the spectra, except for two important differences.

(i) The drop of the frequency ω_A with increasing temperature, also accompanied by a damping of the spectra, is similar, but the position of the step on the temperature scale is shifted to lower temperatures, as shown in Fig. 6.

(ii) Modulation B at room temperature is not damped.

The amplitude effects, however, are the same as for $N_D=8\times10^{17}$ cm^{-3}. A statement about phase shifts cannot be made, as the paired fraction f_{CdP} (and hence the modulation amplitude) is considerably smaller than for $N_D=8\times10^{17}$ cm^{-3}.

For the highest phosphorus concentration ($N_D>10^{18}$ cm^{-3}), PAC spectra at various temperatures are shown in Fig. 7. In comparison to the results at lower N_D's, there is only one striking difference: Except for a slight

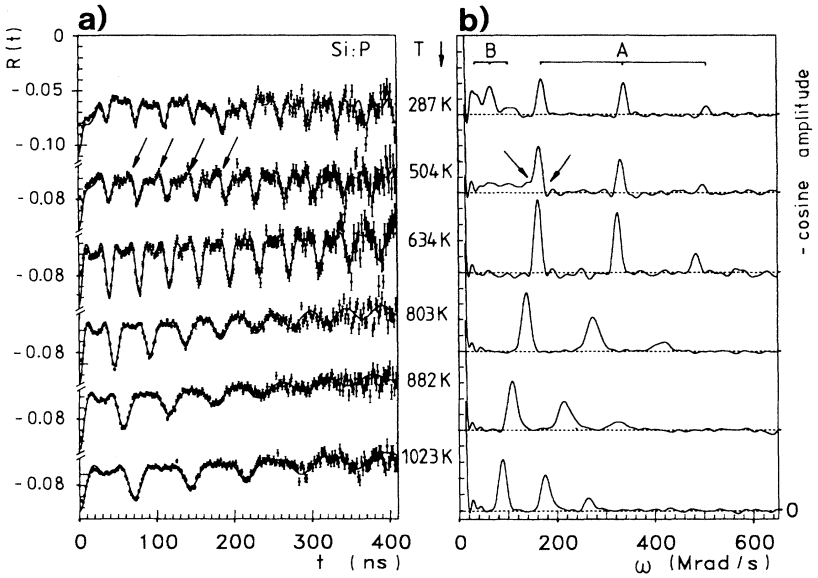

FIG. 5. PAC spectra (a) and cosine-Fourier spectra (b) of ^{111}In/^{111}Cd probe atoms (SDB) in Si:P ($N_D = 8\times10^{17}$ cm^{-3}) at different measuring temperatures. The arrows mark indications of phase shifts relative to pure cosine waves. For the fit curves to the $R(t)$ data, see Sec. V B ($f_{CdD} = 34\%$ except for $T = 1023$ K).

indication in the Fourier spectrum at 287 K, there is no clear evidence of modulation B. Apart from this missing modulation B, the spectra are again similar: The drop of the frequency ω_A is shifted to higher temperature (Fig. 6), again accompanied by a damping of the spectra. Only the first part of the typical steplike shape is observed in the accessible temperature range. Phase shifts are detected in a broad temperature interval around 500 K (see arrows in Fig. 7). The phase shifts in the harmonic frequencies of the triplet occur at higher temperatures than those in the basic wave.

The effect of the donor concentration can be summarized as follows: With increasing N_D, (a) the steplike drop of the frequency ω_A is shifted to higher temperatures, and (b) modulation B (measured at room temperature) becomes damped and finally ($\geq 3\times10^{18}$ cm^{-3}) vanishes completely.[21] The frequency effect (ω_A) and its dependence on N_D has already been reported in Ref. 2. It was successfully explained by the Fermi-level position and the resulting population of two charge states of the CdD pair. Based on this model, the energy level of the pairs is predicted to be close to the middle of the band gap and at $T \leq 500$ K EFG A is ascribed to the negative charge state (CdP)$^-$. As only the ω_A data were used in that study, only a crude upper limit of 72 MHz for the EFG strength of the (CdP)^0 state could be derived. EFG B (36 MHz) is therefore a possible candidate for the (CdP)^0 state. This previous model explaining the ω_A data is a consistent part of the more detailed model presented in this contribution (Sec. VI).

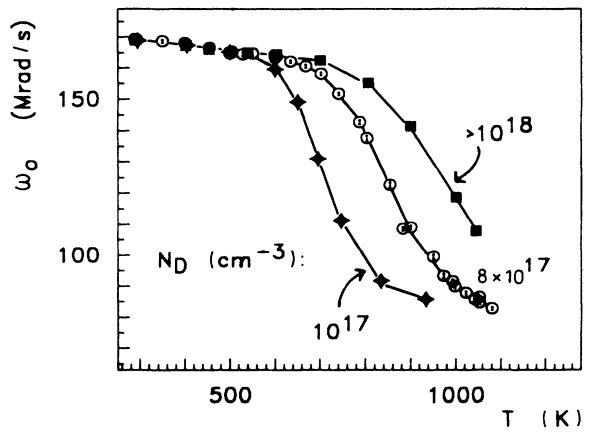

FIG. 6. Basic modulation frequency ω_A of the modulation A in Si:P as a function of temperature at different donor concentrations N_D.

B. Schottky diode experiments

Both the temperature dependence of the spectra (see Sec. V A and Ref. 2) and a naive valency consideration (CdP = double acceptor + single donor = single acceptor ?) lead to the idea that the CdP pairs are electrically active, i.e., the two states characterized by EFG's A and B are different charge states of the same pair. To check this idea, CdP pairs in a Schottky diode were investigated. By variation of the reverse bias of such a device, the depth w of the space-charge region in the semiconductor and hence the population of electronic levels in this region can be influenced. With increasing reverse bias at a Schottky diode on n-type Si, electronic levels are shifted above the Fermi level; i.e., compared to equilibrium conditions charge states containing less electrons are favored. For a detailed description of Schottky contacts and their properties, see Refs. 22 and 23.

These Schottky diode experiments are seriously aggravated by two strongly contradicting experimental restrictions. First, the probe atoms have to be close to the sur-

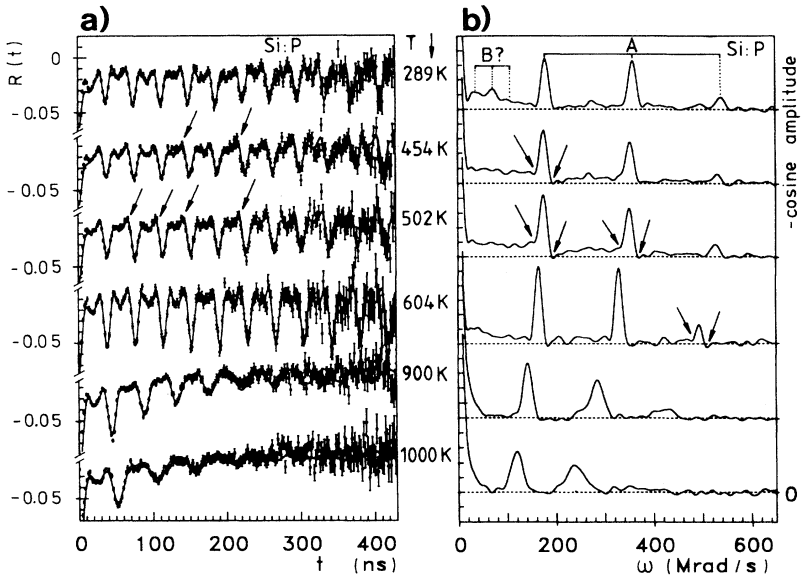

FIG. 7. PAC spectra (a) and cosine-Fourier spectra (b) of ^{111}In/^{111}Cd probe atoms (implanted) in Si:P ($N_D > 10^{18}$ cm^{-3}) at different measuring temperatures. The arrows mark indications of phase shifts relative to pure cosine waves. For the fit curves to the $R(t)$ data, see Sec. VI B ($f_{CdD} = 38\%$).

face and thus must be implanted. Under this circumstance, a phosphorus concentration of at least some 10^{17} cm^{-3} is necessary in order to achieve a minimum detectable fraction f_{CdP} of paired probe atoms.[24] On the other hand, the quality of a Schottky diode deteriorates if N_D increases above 10^{17} cm^{-3}. As a consequence, only an extremely small fraction of probe atoms ($\approx 4\%$) is involved in pairs, and the expected effects in the spectra are very small. The best compromise was found by implanting phosphorus (140 keV, fluence 8×10^{12} cm^{-2}) and ^{111}In (400 keV, $\sim 10^{12}$ cm^{-2}) into low n-doped epi-Si (Sec. III). The pair formation was performed during a thermal annealing process with temperature decreasing from 1000 to 890 K within 24 h, and a Schottky contact was formed by gold evaporation onto the implanted area.

The observed capacitance-voltage (CV) and current-voltage characteristics revealed the typical characteristics of a diode. PAC spectra were taken at room temperature at different reverse bias voltages, and are shown in Fig. 8 for two samples. For each voltage, the depth w of the space-charge region is calculated[23] from the CV data and is given in the figure. It varies between less than 100 nm for $U = 0$ and roughly 200 nm for the highest applied voltage. This ensures that the extension of the space-charge region was indeed shifted across an appreciable part of the probe atoms ($> 60\%$). A slight modulation corresponding to EFG A of the CdP pairs can be found in all spectra without correlation to the applied voltage. With increasing reverse bias, a slight dip in the spectra at $t = 185$ ns is visible, indicated by arrows in Fig. 8. This time exactly corresponds to the modulation period of EFG B of the CdP pairs ($\nu_Q = 36$ MHz). Because of the unavoidably small amplitudes of the spectra, it is hard to

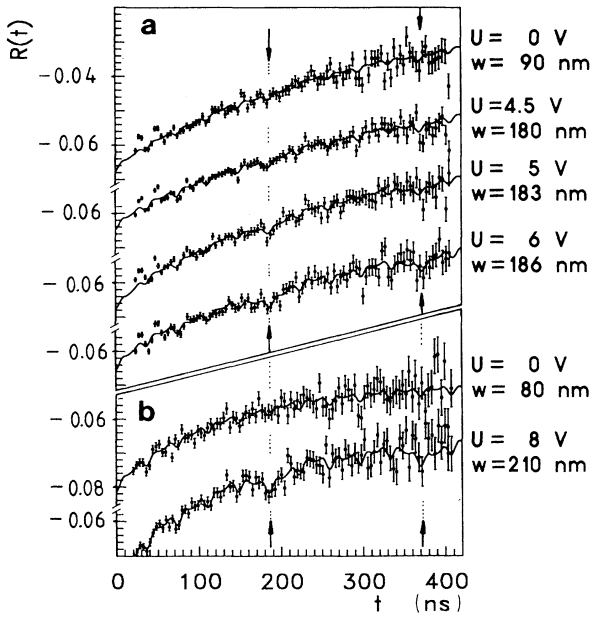

FIG. 8. PAC spectra of two different Schottky contact samples (a) and (b) at different reverse bias voltages at the contact (at $T = 293$ K). For each spectrum, the depth w of the space-charge region (extracted from CV data of the contacts) is given. The arrows mark the modulation period (185 ns) expected for EFG B ($\nu_Q^{(B)} = 36$ MHz). The fit curves correspond to an empirical description with two static EFG's A and B.

prove the occurrence of this EFG rigorously. As the existence of such an EFG at CdP pairs is already known, however, the spectra provide an indication of an increased population of the corresponding state in the Schottky diode experiment. Such a dependence on the electrical potential implies that the CdP pair is electrically active, and state B contains less electrons than state A.

VI. ELECTRONIC PROPERTIES OF Cd-DONOR PAIRS

In this section, we first present a model of the Cd-donor pairs together with its qualitative foundation. Subsequently, the quantitative data evaluation is described, and its results discussed in terms of ordinary semiconductor theory. Finally, a critical discussion and possible extensions of the model are provided.

A. Model of the CdD pair

Based on experimental results, the following model is proposed: The Cd-donor pair CdD (D=P,As,Sb) in silicon forms an electrically active deep center with two charge states labeled $(\mathrm{Cd}D)^-$ and $(\mathrm{Cd}D)^0$.[25] Both states are characterized by axially symmetric EFG's (z axis=$\langle 111\rangle$). In the case of phosphorus, the EFG strength is $\nu_Q^{(1)}=180$ MHz for $(\mathrm{CdP})^-$ and $\nu_Q^{(2)}=36$ MHz for $(\mathrm{CdP})^0$ at room temperature (Table II). The EFG strengths are only slightly temperature dependent ($\approx -10^{-2}$ MHz/K).

This model is justified by the following arguments: The existence of two different states is revealed by the annealing experiments (Sec. IV). The interpretation in terms of charge states and the assignment of $(\mathrm{CdP})^-$ and $(\mathrm{CdP})^0$ to $\nu_Q^{(1)}$ and $\nu_Q^{(2)}$, respectively, is favored by the Schottky diode experiments. Additionally, this interpretation is strongly confirmed by the dependence of the modulation frequency ω_A on temperature and doping (Fig. 6). The $\omega_A(T,N_D)$ data are completely explained by the equilibrium charge state of a CdD level near the center of the band gap.

(a) At $T<600$ K, the Fermi energy is far above the CdP level. Consequently $(\mathrm{CdP})^-$ is a static state. In the PAC spectra, this situation is reflected by an undamped modulation A, whose frequency ω_A directly yields the EFG strength $\nu_Q^{(1)}$ [Eq. (1)]. The slight decrease of $\nu_Q^{(1)}$ with temperature (Fig. 6, $T<600$ K) can be described by a linear approximation:

$$\nu_{Q1}(T)=\nu_{Q1}(0)(1-\alpha T) \quad \text{with } \alpha=8(\pm 1)\times 10^{-5}\ \mathrm{K}^{-1}\ . \tag{23}$$

It is most probably due to thermal lattice vibrations and is independent of N_D.

(b) At temperatures near and above the onset of intrinsic conduction (and hence at an N_D-dependent temperature), the Fermi energy shifts toward the center of the band gap. For a level in this energy range, this results in a decreasing ionization probability and a dynamic equilibrium between the partially occupied states $(\mathrm{CdP})^-$ and $(\mathrm{CdP})^0$. In comparison to Fig. 1, the PAC spectra imply that the transition rate is high enough to fulfill the condition of the "fast fluctuation regime" (Sec. II): the spectra show one damped modulation, whose frequency ω_A directly reflects the decrease of the ionization probability p_1 according to Eq. (20).

This explanation is the only obvious way to explain the ω_A data. They cannot be explained by purely thermal effects because of their N_D dependence. Structural effects, e.g., the lattice expansion due to high doping concentrations, or the thermal lattice expansion, are much too small to explain the data. A direct HFI between the probe atoms and the unpaired donor atoms (only 10^{-3} or less of the donors are involved in pairs) must be excluded because of the short range of the HFI.

All the other effects, i.e., the existence of modulation B, the amplitude effects, and the phase shifts of modulation A, are exactly reproduced by the simulation of Fig. 2. In the context of the proposed model, this means an initial occupation of the nonequilibrium state $(\mathrm{CdP})^0$, whose depopulation occurs during the PAC time window. The transition rate to the equilibrium state [$=(\mathrm{CdP})^-$ at $T<600$ K] increases with temperature. The occupation of the nonequilibrium charge state is a consequence of the preceeding ^{111}In decay. Details of this process will be discussed later.

B. Details of data analysis

Quantitative results about dynamic properties in the context of the proposed model are derived by a fit of the perturbation function $G(t)$ calculated in Sec. II to the $R(t)$ spectra. There are two remarks concerning the applicability of this theory to the CdD pairs.

(a) Though, under (nearly) static conditions (at room temperature), both EFG's of the CdD pair are found to have their largest component (z axis) in the equivalent $\langle 111\rangle$ directions of the Si lattice, it is still an assumption that for an individual pair both EFG's have the same principal-axes system. This assumption, however, is very reasonable; otherwise there would be discrepancies to the data.

(b) The values given for the coupling constants $\nu_Q^{(1)}$ and $\nu_Q^{(2)}$ have, up to now, been understood to be absolute values, as the standard γ-γ PAC under static conditions is not sensitive to their sign. In the dynamic theory, however, the relative sign of the two coupling constants is of importance. Therefore the whole data valuation has to be done with both possibilities of the relative sign, choosing arbitrarily $\nu_Q^{(1)}>0$.

Under these circumstances, a fit of the dynamic perturbation function [together with Eq. (22)] should yield the dynamic parameters of the two-state model, namely the ionization probability p_1, the initial probability p_{1_0}, and the transition rate between the two states. For the convenience of the physical discussion, we choose the rate γ_2 as the independent variable [the other rates γ_1 and γ are directly related to γ_2 by Eq. (4)]. The other parameters can be treated as constants.

(a) Except for the sign problem, $\nu_Q^{(1)}$ and $\nu_Q^{(2)}$ values are known. A slight temperature dependence according to Eq. (23) is used across the whole temperature range.

(b) The fraction $f_{\mathrm{Cd}D}$ of the paired probe atoms is a constant for each sample for all temperatures below the dissociation limit.

This procedure yields excellent fits to the data as shown in Fig. 5 and Fig. 7. The relative sign of the coupling constants cannot be derived from the quality of the fit. The choice of sign, however, influences the results of parameters p_1 and γ_2. This will be discussed below.

C. Shockley-Read statistics

For a physical interpretation of the results which will be presented in the next part of this section, we give a short introduction to the Shockley-Read statistics.[26,27] In Fig. 9, the four different processes for the transition of a charge carrier between a level in the band gap and the bands are shown. They are usually labeled by "*e*" for emission or "*c*" for capture, and "*n*" or "*p*" for electrons or holes, respectively. The rate of a capture process is proportional to the concentration of the species to be captured; the rate for an emission process is essentially given by the Boltzmann factor containing the energy of the level. In the discussion of the experimental results, we will concentrate on the transition $(CdP)^0 \rightarrow (CdP)^-$, which occurs via a *cn* or an *ep* process. Consequently the rate γ_2 of this transition is a sum of the individual rates r_{cn} and r_{ep}:

$$\gamma_2 = r_{cn} + r_{ep} , \tag{24}$$

$$r_{cn} = \sigma_n v_n c_n , \tag{25}$$

$$r_{ep} = \sigma_p v_p g^{-1} N_V \exp\left[-\frac{E_T - E_V}{kT} \right] , \tag{26}$$

where v_x is the thermal velocity of the charge carriers ($x = n,p$), c_n the electron concentration, N_V the effective density of states of the valence band, g the degeneracy factor, and E_T the energy of the level. σ_n and σ_p are the cross sections for the transitions to or from the two bands.

The four possible transition processes lead to an equilibrium probability p_1 for the $(CdP)^-$ state which is given by the Fermi function

$$p_1 = \frac{1}{1 + g \exp[(E_T - E_F)/(kT)]} . \tag{27}$$

In the context of this statistical description, the microscopic mechanism of the transition processes is contained in the cross sections. Depending on the type of the mechanism (or on the kind of impurity), cross sections between 10^{-18} and 10^{-11} cm^2 are reported.[28] The mechanisms discussed most frequently are the multiphonon process and the cascade capture.[27] The expected temperature dependences of these processes are $\exp(-1/T)$ and T^{-m}, respectively. For the exponent m in the power law, values between 0 and 4 are reported.[28] At high carrier concentrations an additional mechanism, the Auger effect, may contribute to the cross section of the majority carriers, as in this case σ is proportional to the carrier concentration. Summarizing these facts, there is no reasonable way to predict the T dependence of the cross sections of the Cd*D* pairs. For practical reasons, a power law (T^{-m}) will be used during the data evaluation, leaving the exponent m unknown in the interval [0,4].

Regardless of this difficulty, Eqs. (25) and (26) imply a characteristic dependence of the γ_2 rate on the experimentally varied parameters T and N_D, which will be important for the identification of these processes: The rate of the electron capture process (*cn*) is governed by the electron concentration c_n. For an extrinsic semiconductor (with complete ionization of the dominant doping impurity), c_n is equal to N_D and thus independent of temperature; for the samples of the present experiments, this statement is true at temperatures between 300 and at least 750 K. On the other hand, an emission process is dominated by the Boltzmann factor and thus independent of N_D.

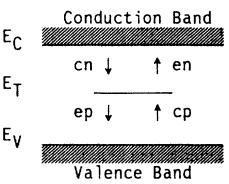

FIG. 9. Schematic illustration of the charge transitions at a level in the band gap of a semiconductor. In the labels of the four processes, "*e*" denotes emission, "*c*" means capture, and "*n*" or "*p*" refer to electrons or holes, respectively.

D. Results and discussion

The results of the equilibrium ionization probability p_1 are shown in Fig. 10, assuming $\nu_Q^{(2)} > 0$. For $\nu_Q^{(2)} < 0$, the decrease of the p_1 values is smaller (from 1 down to 0.55) but qualitatively the same. According to Eq. (20), the p_1 data can be understood as a rescaling of the $\omega_A(T)$ data of Fig. 6. As already discussed in Sec. VI A, the results can be explained by the position of the Fermi level E_F together with Eq. (27). As E_F can be calculated for given T and N_D, the trap parameters E_T and g can be obtained from a fit of this equation to the p_1 data. For the sample doped by P implantation, N_D is treated as a free fit parameter; the result is 3×10^{18} cm^{-3}. The uncertainty of the $\nu_Q^{(2)}$ sign mainly affects the extracted degeneracy factor g. For $\nu_Q^{(2)} < 0$, the fit yields extremely small g factors ([0.05;0.4]); as g should be of order unity, this possibility

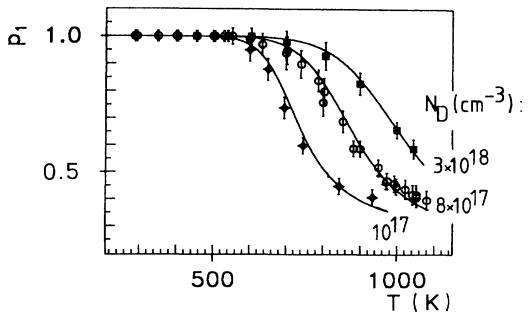

FIG. 10. Equilibrium probability p_1 of the $(CdP)^-$ state for different donor concentrations N_D. The values are extracted under the assumption of an identical sign of $\nu_Q^{(1)}$ and $\nu_Q^{(2)}$. The curves are fits of Eq. (27) to the data ($g = 1$, $E_T = E_V + 0.5$ eV).

seems rather unlikely. This argument, however, cannot be used to rule out the possibility of $\nu_Q^{(2)}<0$ completely, because such extreme g factors have been reported for other impurities, as well [e.g., Au in Si (Ref. 29)]. For $\nu_Q^{(2)}>0$, the extracted g factors are uncertain within the range [0.2;2]; due to the large spread no useful information can be obtained from this parameter. The more important parameter, the trap energy E_T, turns out to be rather insensitive to all uncertainties and is determined to be 0.55 ($\pm$0.10) eV above the valence band.

The ionization probability at the time zero of the HFI, p_{1_0}, is found to be 0.4$\pm$0.1 for all spectra at $T_m<600$ K, without significant dependence on temperature or doping (without figure). At higher temperatures, the parameter p_{1_0} cannot be obtained from the spectra, as the transition rate becomes too high ($\Gamma_0 \gg 1$), and thus p_{1_0} has no influence on $G(t)$.

The nonequilibrium state ($p_{1_0} \neq p_1$) at $t=0$ is a consequence of the preceeding decay $^{111}\text{In} \rightarrow {}^{111}\text{Cd}$. The electron-capture (EC) decay and subsequent x-ray and Auger processes create a multiply charged, highly excited positive Cd ion,[8] which relaxes by capture of electrons from the surrounding crystal. Taking into account the time scale of the PAC measurement, the relaxation may be divided into two steps.

(a) Fast relaxation without influence on the PAC spectra, i.e., within less than 1 ns (corresponding to $\Gamma_0 \gg 1$). The parameter p_{1_0} describes the probability that these fast processes already result in an occupation of the equilibrium state ($p_1=1$ at $T<600$ K). Because of the short duration of these processes, the missing influence of temperature on p_{1_0} seems reasonable (the relevant processes are faster than a typical phonon frequency or at least than a phonon lifetime).

(b) Slow processes taking place during the observable time window of the HFI, i.e., within roughly 0.5 μs.

The whole relaxation process is an extremely complicated matter which covers many orders of magnitude both on time and energy scales. The assumption that all but the final transition $(\text{CdP})^0 \rightarrow (\text{CdP})^-$ belongs to the first group results in a consistent explanation of the data. In the simplest version of a subsequent filling of empty electron states, this idea results in $p_{1_0}=0$. The observed value $p_{1_0}=0.4$ may be explained by a locally enhanced electron concentration due to the short-lived positive center which drives the charge state p_{1_0} closer to the equilibrium value $p_1=1$. In this model, only transitions at a level in the band gap are slow enough to be directly observed by PAC. This is coincident with other PAC experiments: So-called "after-effects" of the preceding decay are reported for a number of electrically active centers, e.g., Cd in Si,[30] Cd in Ge, and Cd in SnO_2, but not in ZnO,[31] where Cd is isoelectronic and thus is not expected to have a level in the band gap. In these examples, however, no quantitative description of the after-effect has been given, and the initial state has not been specified. Similar effects are reported[32] from Mössbauer spectroscopy at the probe atom $^{129}\text{Te}/^{129}\text{I}$.

All these statements about the p_1 and p_{1_0} data, including the extracted trap energy, are also true for the CdAs and CdSb pair in silicon.

The results of the transition rate γ_2 are shown in Fig. 11. Because of their characteristic dependence on T and N_D (see the discussion in Sec. VI C) the two processes *ep* and *cn* contribute in the following way to the total rate γ_2.

(a) At high temperatures (>500 K), the *ep* process is dominant; this results in the exponential T dependence of the data regardless of sample doping.

(b) At low temperatures, the *cn* process dominates; the data depend on N_D and are nearly independent of temperature.

This identification can be used for a quantitative evaluation of the γ_2 data by fitting them with a theory function according to Shockley-Read statistics [Eqs. (24)–(26)]. In principle, the trap energy E_T is determined by the slope of the Arrhenius plot in Fig. 11; due to the uncertainty in the T dependence of σ_p, however, the extracted values are uncertain within a broad interval (0.2 eV for $m=0$, 0.45 eV for $m=4$, if $\sigma_p \propto T^{-m}$). This interval nearly overlaps with the result $E_T=0.55$ ($\pm$0.10) eV (relative to the valence band) obtained from the p_1 data. As the slope in an Arrhenius plot contains an entropy term in addition to the trap energy, the values from the p_1 and the γ_2 data are not expected to be absolutely identical. The E_T value obtained from the p_1 data is more reliable. The cross section σ_n is easily obtained from the low-temperature data [Eq. (25), $c_n=N_D$ in the relevant temperature range]; the result is $\sigma_n=1.2\ (\pm 0.4)\times 10^{-18}$ cm^2.

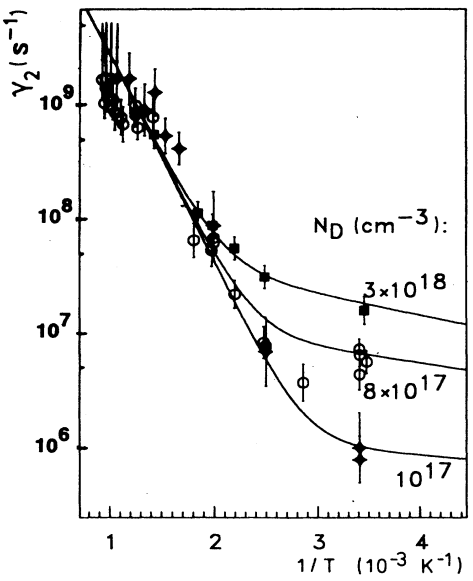

FIG. 11. Transition rate γ_2 [$(\text{CdP})^0 \rightarrow (\text{CdP})^-$] at CdP pairs in Si for different donor concentrations N_D, extracted under the assumption of an identical sign of $\nu_Q^{(1)}$ and $\nu_Q^{(2)}$. The curves are calculated by Shockley-Read statistics [Eqs. (24)–(26)] with the trap parameters $g=1$, $E_T=E_V+0.4$ eV, $\sigma_n=10^{-18}$ cm^2, $\sigma_p \propto T^{-3}$, and $\sigma_p(800\text{ K})=10^{-16}$ cm^2.

The cross section σ_p is strongly influenced by its assumed T dependence; at 800 K, the order of magnitude is 10^{-16} cm^2.

The γ_2 data of the other pairs, CdAs and CdSb, do not exhibit the structure of a superposition of a *cn* and a *cp* process as clearly as the data of the CdP pair. There is also a low-temperature behavior consistent with a *cn* process, but at high temperatures the increase of the γ_2 values is not pronounced enough to prove strongly the existence of the *ep* process. Taking the trap energy E_T from the p_1 data and using Shockley-Read statistics, the data are consistently explained by the same model as that for the CdP pair, i.e., by a superposition of a *cn* (low T) and an *ep* process (dominant at high T). The results for the cross sections are the same, as well.

The identification of the dominant process (*cn*) at room temperature explains the mystery of the missing modulation B in the spectra of samples with a very high donor concentration (Sec. IV): at room temperature, the transition rate γ_2 is proportional to N_D; according to the dynamic PAC theory of Sec. II, it is equal to the damping constant of modulation B. Therefore this modulation is no longer observable if N_D (and thus the damping constant) exceeds a critical value.

A striking confirmation of the present model comes from PAC experiments[7] starting with ^{111m}Cd instead of ^{111}In: pair formation experiments (all measurements at room temperature) in Si:P and Si:As reveal (among others) the EFG's which are assigned to the equilibrium state $(CdD)^-$ in the present paper. The EFG's of the $(CdD)^0$ state are not observed. As these experiments do not involve an elemental transmutation (and subsequent after-effects), this result strongly confirms our interpretation that $(CdD)^0$ is populated as a consequence of the preceding ^{111}In decay in the present experiments.

Summarizing this subsection, we find that the equilibrium dynamic variables p_1 and γ_2 are consistently explained by the Shockley-Read statistics without further assumptions; and basic trap parameters are derived. The initial probability p_{1_0} is the final result of an extremely complicated relaxation process initiated by the ^{111}In decay; a very simple model yields at least a reasonable explanation which is consistent with other experiments.

If we rely on the more reasonable choice of an identical sign of the coupling constants of both states, there is a remarkable common ground of the three CdD pairs: the difference $\nu_Q^{(1)} - \nu_Q^{(2)}$ is nearly identical [$= 145\ (\pm 3)$ MHz]. This fact possibly indicates a simple explanation for the strength of the EFG's: each CdD pair results in an EFG increasing with the size of the donor, but independent of the charge state; the capture of an additional electron switches on an additional EFG (145 MHz) regardless of the type of donor.

E. Comments and extensions of the model

The two-state model is the simplest choice which consistently explains all experimental data. In this subsection we discuss magnetic interaction, general consequences for PAC spectroscopy, and possible extensions of the model to excited states of the center.

The two-state model $[(CdP)^-/(CdP)^0]$ implies that one of the two states should have an unpaired electron and thus should be paramagnetic. In principle, a magnetic HFI between this electron and the magnetic moment of the probe nucleus is to be expected. In the spectra, however, there is no indication of a magnetic HFI: the modulations are perfectly described by fluctuating EFG's and the nonmodulated part of the spectra is constant though the occupation of the two states changes markedly. A possible solution to this problem within the framework of the model is that the magnetic HFI is too weak to have a detectable influence. This can be understood if the orbital of the unpaired electron is not localized directly at the Cd atom. This proposal is not in contradiction to the fact that the capture of an additional electron in this orbital strongly changes the EFG: this EFG difference is not necessarily due to the direct electrostatic HFI of this electron with the probe nucleus, but may be caused by secondary effects (e.g., a change of the Cd-P bond length) as well. This argument illustrates only a possible explanation for the missing magnetic HFI; it is, of course, definitely impossible to derive the spatial charge distribution from measured EFG's.

The possibility that both the charge state as well as dynamic processes (including decay after-effects) may have strong effects on the PAC spectra must be carefully taken into account during the data analysis of PAC spectra of semiconductors. Neglecting these effects may lead to serious errors in the interpretation. This may be illustrated by an example: in former PAC studies[19,20] (on the same probe atom) concentrating on the ^{111}In-donor pair formation, the spectra had been analyzed assuming a static HFI (and neglecting modulation B); as a consequence, the extracted result, the fraction of paired probe atoms, is too small by a factor of at least 2.5. As all measurements of that study had been performed at room temperature, the measured spectra really do not exhibit any direct evidence of dynamic effects. This example demonstrates that dynamic effects may seriously influence the spectra without leaving a characteristic fingerprint, and thus may lead to a misinterpretation. This source of errors may be minimized by investigating a broad range of measuring conditions.

As an extension of the proposed model, excited states may be taken into account. The equilibrium occupation of the ground state is not influenced by such states, if they are separated from the ground state by an energy $\Delta E \gg kT$. Nonequilibrium effects, however, especially the capture of charge carriers, may occur along a ladder of excited states. This so-called cascade capture has strong effects on the capture rate and is one of the most frequently discussed capture mechanisms.[27,29] In the case of such a cascade capture, there is one important point concerning the interpretation of capture rates: "classical" methods (involving the measurement of electronic transport properties) as well as theoretical calculations always refer to the capture from a band state to any bound state, not necessarily to the ground state. From the point of view of PAC spectroscopy, however, the EFG of the excited states is certainly different from that of the ground state; furthermore, it may even be identical to

that of the unbound state, because excited states are expected to be less localized than the ground state and the range of the HFI is very short. In this case, the rate determined by PAC refers to the transition to the ground state.

In the present experiments on CdD pairs, the existence of excited states cannot be excluded, but there is no evidence of serious influence as all data are completely explained by only two states. To solve this question, both PAC data and results from "classical" methods of the same trap are necessary, as the cascade model predicts a large difference between the observed rates.

VII. CONCLUSIONS

Dynamic processes at a PAC probe atom can be analyzed quantitatively. For a two-state system with fluctuating strength of the electric hyperfine interaction, the perturbation function presented in this paper enables the determination of transition rates and occupation probabilities, including relaxation effects. If the PAC probe atom forms (or is part of) an electrically active defect in a semiconductor, the transitions between its charge states are observed directly. The basic requirements are as follows.

(a) There must be a nonstatic charge state of the level, caused either by nonequilibrium effects or by partial occupation of the level, i.e., an ionization probability different from 0 or 1.

(b) The transition rates should be in the proper order of magnitude; this can be expressed generally by the condition $0.01 < \Gamma_0 < 100$. For the examples in this paper and ^{111}Cd probe atoms, this corresponds to rates between 10^6 and 10^{10} s^{-1}.

(c) The charge distribution is changed directly at the probe atom (within a few atomic distances). For a shallow level with hydrogenlike orbitals extending over many atomic distances, no influence on the EFG at the probe atom is expected. In this context the method is restricted to "deep" levels with a strongly localized orbital. Furthermore, the EFG at the probe atoms must not vanish from symmetry considerations; this requirement excludes a study of isolated (i.e., unpaired) probe atoms in cubic semiconductors.

(d) The EFG's of the two static charge states should be known, including strength, symmetry, and orientation. Otherwise the results will be less accurate.

Under these conditions, the elementary process of a carrier recombination or emission at a trap, i.e., the change in the charge distribution at this trap, can be studied on a nanosecond time scale. In this sense, the PAC method is complementary to classical techniques, which are sensitive to the consequences of this process on electronic parameters of the semiconductor. The ability to measure the transition rate at a trap even in thermal equilibrium is a unique feature of this PAC application.

By a combination of different methods in future experiments at the same trap, this complementarity may be used to investigate the capture mechanisms in great detail. The difference between rates measured by PAC and those measured by "classical" methods depends critically on the capture mechanism. Thus a sensitive experimental test for the validity of capture models should be possible.

The Cd-donor pairs in silicon investigated here are found to form a deep trap close to the center of the band gap. The most relevant trap parameters are derived; within experimental errors, the properties of the pairs are the same for the three donors P, As, and Sb. A similar PAC study, using the perturbation function presented here, has been done for the Cd-hydrogen pair in silicon;[33,34] it forms a comparatively shallow acceptor level.

ACKNOWLEDGMENTS

We thank Dr. M. Uhrmacher (University of Göttingen) for the radioactive ^{111}In implantations and Dr. G. Pensl (University of Erlangen) for P and Sb implantations of several samples. This work has been funded by the German Federal Minister for Research and Technology under Contract No. CHR2ERL.

[1]D. Forkel, W. Engel, M. Iwatschenko-Borho, R. Keitel, and W. Witthuhn, Hyperfine Interact. **15/16**, 821 (1983).

[2]N. Achtziger, S. Deubler, D. Forkel, H. Wolf, and W. Witthuhn, Appl. Phys. Lett. **55**, 766 (1989).

[3]A. Baurichter, S. Deubler, D. Forkel, M. Gebhard, H. Wolf, and W. Witthuhn, Mater. Sci. Eng. B **4**, 281 (1989).

[4]H. Skudlik, M. Deicher, R. Keller, R. Magerle, W. Pfeiffer, D. Steiner, E. Recknagel, and Th. Wichert, Phys. Rev. B **46**, 2159 (1992); see also Ref. 13.

[5]N. E. B. Cowern, Appl. Phys. Lett. **54**, 703 (1989).

[6]N. Achtziger *et al.* (unpublished).

[7]D. Steiner, M. Deicher, R. Keller, W. Pfeiffer, H. Skudlik, and Th. Wichert (unpublished).

[8]H. Frauenfelder and R. M. Steffen, in *Alpha-, Beta-, Gamma-Ray Spectroscopy,* edited by K. Siegbahn (North-Holland, Amsterdam, 1965).

[9]H. H. Rinneberg, At. Energy Rev. **172**, 477 (1979).

[10]W. E. Evenson, A. G. McKale, H. T. Su, and J. A. Gardner, Hyperfine Interact. **61**, 1379 (1990).

[11]H. Winkler and E. Gerdau, Z. Phys. **262**, 363 (1973).

[12]N. Achtziger, Ph.D. thesis, Universität Erlangen-Nürnberg, 1991.

[13]In Ref. 4, the perturbation function for fast fluctuations of the EFG strength is incorrect. The equation stated there applies to fluctuating orientation (but constant strength) only.

[14]J. C. Hamilton, *The Electromagnetic Interaction in Nuclear Spectroscopy* (North-Holland, Amsterdam, 1975).

[15]G. Schatz and A. Weidinger, *Nukleare Festkörperphysik* (Teubner, Stuttgart, 1985).

[16]Th. Wichert, M. Deicher, G. Grübel, R. Keller, N. Schulz, and H. Skudlik, Appl. Phys. A **48**, 59 (1989).

[17]Th. Wichert, N. Achtziger, H. Metzner, and R. Sielemann, in *Hyperfine Interaction of Defects in Semiconductors,* edited by G. Langouche (North-Holland, Amsterdam, 1992).

[18]R. Lindner, R. Helbig, V. Lehmann, R. Hoffmann-Tikkanen, and P. A. Glasow, in *Magnetic Thin Films, Multilayers and Superlattices,* European Materials Research Society Symposium Proceedings Vol. XVI (North-Holland, Amsterdam,

1987), p. 373.
[19]M. L. Swanson, Th. Wichert, and A. F. Quenneville, Appl. Phys. Lett. **49**, 265 (1986).
[20]Th. Wichert and M. L. Swanson, J. Appl. Phys. **66**, 3026 (1989).
[21]This statement includes all samples of the present experiments and of Ref. 20.
[22]E. H. Rhoderik, *Metal-Semiconductor Contacts* (Clarendon, Oxford, 1978).
[23]B. L. Sharma, *Metal-Semiconductor Schottky Barrier Junctions and Their Application* (Plenum, New York, 1984).
[24]For the other donors, As and Sb, the pair formation is even less pronounced than for phosphorus, and Schottky experiments are not possible.
[25]As the PAC spectroscopy is not sensitive to the absolute charge state, these labels—for the moment—are to indicate only that $(CdP)^-$ contains one more bound electron than $(CdP)^0$.
[26]W. Shockley and W. T. Read, Phys. Rev. **87**, 835 (1952).
[27]V. N. Abakumov, V. I. Perel, and I. N. Yassievich, *Nonradiative Recombination in Semiconductors* (North-Holland, Amsterdam, 1991).
[28]V. L. Bonch-Bruevich and E. G. Landsberg, Phys. Status Solidi **29**, 9 (1968).
[29]A. G. Milnes, *Deep Impurities in Semiconductors* (Wiley, New York, 1973).
[30]M. Deicher, G. Grübel, E. Recknagel, Th. Wichert, and D. Forkel, Nucl. Instrum. Methods B **13**, 499 (1986).
[31]D. Forkel, Ph.D. thesis, Universität Erlangen-Nürnberg, 1987.
[32]G. J. Semerink, H. de Waard, L. Niesen, and D. O. Boerma, Hyperfine Interact. **14**, 53 (1983).
[33]M. Gebhard, N. Achtziger, A. Baurichter, D. Forkel, B. Vogt, and W. Witthuhn, Physica B **170**, 320 (1991).
[34]M. Gebhard, Ph.D. thesis, Universität Erlangen-Nürnberg, 1992.